A Theoretical Study on the Two Reactions of Acetonitrile with Atomic Chlorine and Bromine

Qian Shu Li*,†,‡ and Chao Yang Wang†

School of Chemical Engineering & Materials Science, Beijing Institute of Technology, Beijing 100081, P. R. China, and Institute of Theoretical Chemistry, State Key Laboratory of Theoretical and Computational Chemistry, Jilin University, Changchun 130023, P. R. China

Received: December 10, 2001; In Final Form: June 28, 2002

The two reactions of acetonitrile with atomic chlorine and bromine have been studied using the density functional theory method. By comparing with the available experimental data and quadratic configuration interaction results, the combination of the hybrid Becke's half-and-half method for nonlocal exchange and the Lee−Yang−Parr nonlocal correlation functional method (BH&HLYP) with the 6-311G(d, p) basis set is settled on the minimum energy paths calculations for the two reactions. Barrier heights for the two forward reactions are predicted theoretically to be 5.36 and 13.03 kcal mol^{-1} at the BH&HLYP/6-311++G(3df, 2p)// BH&HLYP/6-311G(d, p) level, respectively. The canonical variational transition state theory incorporating the zero-curvature tunneling and small-curvature tunneling corrections using the general polyatomic rate constant code Polyrate-8.2 was used to predict the rate constants of the two reactions. The calculated rate constants and the activation energies for the reaction of acetonitrile with chlorine atom are in satisfactory agreement with the experimental data in the temperature range from 250 to 723 K.

1. Introduction

Experimental observations of positive ions in the stratosphere[1−3] have shown the presence of acetonitrile (CH_3CN)[4−6] coming mainly from various combustion processes,[7,8] including biomass burning, internal combustion engines burning and so on. CH_3CN then diffuses into the stratosphere in which it is progressively destroyed through chemical reactions.[9] Early studies showed that the main loss of acetonitrile in the stratosphere is attributed to its reaction with hydroxyl radicals. Later studies showed that the possibility of a supplementary acetonitrile destruction reaction with the chlorine atom[9] may become significant at high altitudes, because it is known that radicals of chlorine and bromine also exist in the atmosphere.

The reaction between acetonitrile and atomic chlorine has been studied experimentally by several authors.[10−13] Olbregts et al.[10] conducted a competitive chlorination experiment at 370 and 413 K, using chloroform as the reference gas. Poulet et al.[11] measured absolute values of the rate constants between 295 and 723 K using a discharge flow tube, with chlorine atoms in excess, and performed mass spectroscopic detection of acetonitrile. The experimental results of Poulet et al. showed a curved Arrhenius plot, with effective activation energies of 6 kcal mol^{-1} at 723 K and 3 kcal mol^{-1} at 295 K. The rate constant determined at room temperature is 9×10^{-15} cm^3 mol^{-1} s^{-1}. Kurylo et al.[12] obtained an upper limit of the rate constant of 2×10^{-15} cm^3 molecule^{-1} s^{-1} at 298 K using flash photolysis with resonance fluorescence detection of chlorine atoms. Tyndall et al.[13] measured the rate constant as $(1.15 \pm 0.20) \times 10^{-14}$ cm^3 mol^{-1} s^{-1} at 296 ± 2 K using laser flash photolysis with the atomic resonance fluorescence technique. But the reaction between acetonitrile and atomic bromine has not been reported to date. An aim of the present paper is to study theoretically the dynamic properties of the reactions of acetonitrile with atomic chlorine and bromine.

Former studies[14−18] suggested that density functional theory (DFT), particularly the BH&HLYP approach can provide sufficient accurate potential energy surface information for rate calculations. BH&HLYP here denotes a combination of the hybrid Becke's half-and-half (BH&H)[19] method for nonlocal exchange and the Lee−Yang−Parr (LYP)[20] nonlocal correlation functional. Its computational advantage would allow the application of the direct dynamics method in the study of reactions involving large polyatomic molecules.

In the present article, a direct dynamics study for the two titled reactions is performed with use of the BH&HLYP/6-311G(d, p) method. The calculated rate constants and the activation energies for the reaction of acetonitrile with chlorine atom are also compared with the available experimental data.

2. Calculation Methods

In the present study, the geometric parameters, energies, and vibrational frequencies of all stationary points for the two titled reactions were computed using the BH&HLYP approach with the 6-31+G(d, p) and 6-311G(d, p) basis sets. MP2 and QCISD methods were also used to calculate the stationary point properties of the reaction CH_3CN+Cl for a comparison. MP2 here denotes the second-order Møller−Plesset perturbation[21,22] theory, and QCISD denotes the quadratic configuration interaction[23] method. The minimum energy paths (MEPs) were calculated at the BH&HLYP/6-311G(d, p) level by the internal reaction coordinate s with a gradient step size of 0.01 (amu)$^{1/2}$ bohr, computing 150 points in the reactant channels [down to $s = -1.50$ (amu)$^{1/2}$ bohr] and 150 points in the product channels [up to $s = +1.50$ (amu)$^{1/2}$ bohr]. Along with the MEPs of each reaction, the intrinsic reaction coordinate s is defined as the

* Corresponding author: qsli@mh.bit.edu.cn.
† Beijing Institute of Technology.
‡ Jilin University.

10.1021/jp0144707 CCC: $22.00
Published on Web 08/24/2002

TABLE 1: Optimized and Experimental Geometrical Parameters (distance in Å, Angle in Degrees) at the Stationary Points

species	geometrical parameters	BH&HLYP 6-311G(d, p)[a]	BH&HLYP 6-31+G(d, p)	MP2 6-311G(d, p)	MP2 6-31+G(d, p)	QCISD 6-311G(d, p)	exptl
CH_3CN	$r(C^1\text{-}H^4)$	1.084	1.085	1.092	1.088	1.093	1.094[b]
$C_{3v}\ ^1A_1$	$r(C^1\text{-}C^2)$	1.453	1.457	1.462	1.463	1.471	1.462[b]
	$rC^2\text{-}N^3$	1.139	1.147	1.173	1.181	1.160	1.156[b]
	$\angle(H^4C^1C^2)$	110.0	109.9	110.0	109.9	109.8	109.7[c]
	$\angle(C^1C^2N^3)$	180.0	180.0	180.0	180.0	180.0	180.0[b]
CH_2CN	$r(C^1\text{-}H^4)$	1.073	1.075	1.079	1.076	1.083	1.089[d]
$C_{2v}\ ^2B_1$	$r(C^1\text{-}C^2)$	1.377	1.381	1.415	1.416	1.400	1.368[d]
	$r(C^2\text{-}N^3)$	1.154	1.163	1.142	1.149	1.175	1.192[d]
	$\angle(H^4C^1C^2)$	119.9	119.9	119.5	119.5	119.8	
HCl	$r(Cl^1\text{-}H^6)$	1.276	1.274	1.273	1.270	1.276	1.275[c]
HBr	$r(Br^7\text{-}H^6)$	1.414	1.407	1.412	1.435	1.416	1.415[c]
NC_2H_2-H-Cl	$r(C^1\text{-}H^4)$	1.079	1.081	1.086	1.083	1.089	
$C_S\ ^2A'$	$r(C^1\text{-}C^2)$	1.416	1.419	1.446	1.447	1.439	
	$r(C^2\text{-}N^3)$	1.144	1.152	1.139	1.145	1.165	
	$r(C^1-H^6)$	1.337	1.345	1.392	1.404	1.335	
	$r(Cl^7-H^6)$	1.497	1.490	1.423	1.418	1.487	
	$\angle(H^4C^1C^2)$	115.3	115.3	115.1	115.0	114.9	
	$\angle(C^2C^1H^6)$	106.7	106.8	105.0	105.0	106.3	
	$\angle(H^4C^1H^5)$	115.3	115.4	115.9	116.0	115.1	
	$\angle(C^1C^2N^3)$	179.1	179.0	179.3	180.0	178.9	
	$\angle(C^1H^6Cl^7)$	174.2	177.1	177.3	178.6	174.0	
	$\tau(H^5C^1C^2H^4)$	138.3	138.4	138.7	139.9	136.9	
	$\tau(Cl^7H^6C^1C^2)$	180.0	180.0	180.0	180.0	180.0	

[a] Calculated geometies at the BH&HLYP/6-311G(d, p) level for the transition state $NCCH_2\cdots H\cdots Br$: $r(C^1\text{-}C^2) = 1.405$; $r(C^2\text{-}N^3) = 1.147$; $r(C^1\text{-}H^3) = 1.078$; $r(C^1\cdots H^6) = 1.482$; $r(H^6\cdots Br^7) = 1.559$; $\angle(H^4C^1C^2) = 116.7$; $\angle(C^1H^6Br^7) = 173.3°$. [b] ref 34. [c] ref 35. [d] ref 36.

signed distance from the saddle point, with $s < 0$ referring to the reactant side. At each selected point along the MEPs, the forces and Hessians were obtained at the BH&HLYP/6-311G(d,p) level. The single-point energy calculations for all stationary points and the selected points along the MEPs were performed at the BH&HLYP/6-311++G(3df, 2p) level for the two reactions. For the reaction of acetonitrile with the chlorine atom, the single-point energy calculations for stationary points were also done at the QCISD(T)/6-311G(d, p)//MP2/6-311G(d, p), QCISD/6-311++G(d, p)//MP2/6-311G(d, p), and CCSD(T)/cc-pVTZ//QCISD/6-311G(d, p) levels, and were performed using the G2 scheme. Note that the G2 calculations were here made with the MP2/6-311G(d, p) geometries and frequencies, respectively. All the calculations above were performed using the Gaussian 98 program suite.[24] Electronic structural information was further used to compute the theoretical rate constants. The rate constants and activation energies at various temperatures were calculated using the conventional transition state theory (TST) and canonical variational transition state theory (CVT) in the Polyrate 8.2 program.[25] The CVT was based on varying the dividing surface along a reference path to minimize the rate constant. Furthermore, the CVT rate constants are corrected with the zero-curvature tunneling (ZCT) and the small-curvature tunneling (SCT)[26−33] transmission coefficient.

3. Results and Discussion

A. Stationary Points. Geometric parameters for the reactant (CH_3CN), products (CH_2CN, HCl and HBr), and the transition states obtained from different theoretical methods are listed in Table 1, along with their experimental values.[34−36] The corresponding structures are displayed in Figure 1. For the reactant and product structures, namely, CH_3CN, CH_2CN, HCl, and HBr, these methods yielded results in excellent agreement with the experimental data. Geometries of CH_3CN and CH_2CN also showed good agreement with the theoretical results obtained by Wang et al.[37] at the B3LYP/6-311++G(2d, 2p) level and Gutsev et al.[38] at the CASSCF/GENCAS level. The largest discrepancies between calculated geometries at different levels were found at the transition state $NCH_2C^1\cdots H^6\cdots Cl.^7$ For the predicted active $C^1\cdots H^6$ and $H^6\cdots Cl^7$ bond distances, the largest discrepancies were both 0.069 Å at the MP2 level with respect to those at the QCISD, whereas the BH&HLYP gave a difference of only 0.01 Å. The angle between the active $C^1\cdots H^6$ and $H^6\cdots Cl^7$ bonds, $C^1\cdots H^6\cdots Cl,^7$ calculated at the BH&HLYP/6-311G(d, p) level was close to that of the QCISD/6-311G(d, p) level only with a difference of 0.2°, whereas the BH&HLYP/6-31+G(d, p), MP2/6-31+G(d, p), and MP2/6-311G(d, p) results were all different from that at the QCISD level by up to 3.1°. Therefore, by comparing with the more accurate ab initio results from the QCISD/6-311G(d, p), it is found that the geometries calculated at the BH&HLYP/6-311G(d, P) level are more reasonable than those of MP2.

The reaction energies and barrier heights of the two reactions are listed in Table 2. In comparison with the experimental reaction enthalpy[39] of -8.31 ± 8.97 kcal mol^{-1}, for the reaction CH_3CN+Cl, it can be seen that the BH&HLYP/6-311++G(3df, 2p)//BH&HLYP/6-311G(d, p) value (-7.26 kcal mol^{-1}) is the closest to the experimental data. However, it is rather surprising that the MP2 completely fails to even predict the sign of the reaction enthalpy, which are 9.23 kcal mol^{-1} at the MP2/6-31+G(d, p) level and 6.47 kcal mol^{-1} at the MP2/6-311G(d, p) level, for this reaction. The reaction energies calculated at the BH&HLYP/6-311G(d, p) and BH&HLYP/6-31+G(d, p) levels were -1.15 and 0.15 kcal mol^{-1}, which were close to 0.27 kcal mol^{-1} at the QCISD/6-311G(d, p) level. However, the values 9.41 and 12.21 kcal mol^{-1} from MP2/6-311G(d, p) and MP2/6-31+G(d, p) are much higher than that from QCISD/6-311G(d, p). The BH&HLYP/6-311++G(3df, 2p)//BH&HLYP/6-311G(d, p) result was -2.05 kcal mol^{-1} more exothermic than the CCSD(T)/cc-pVTZ//QCISD/6-311G(d, p) value. As shown in Table 2, the calculated barrier heights are quite scattered for different methods. The barrier heights calculated using BH&HLYP/6-311++G(3df, 2p)//BH&HLYP/6-311G(d, p) method is 5.36 kcal mol^{-1}, which is close to that using CCSD(T)/cc-PVTD//QCISD/6-311G(d, p)

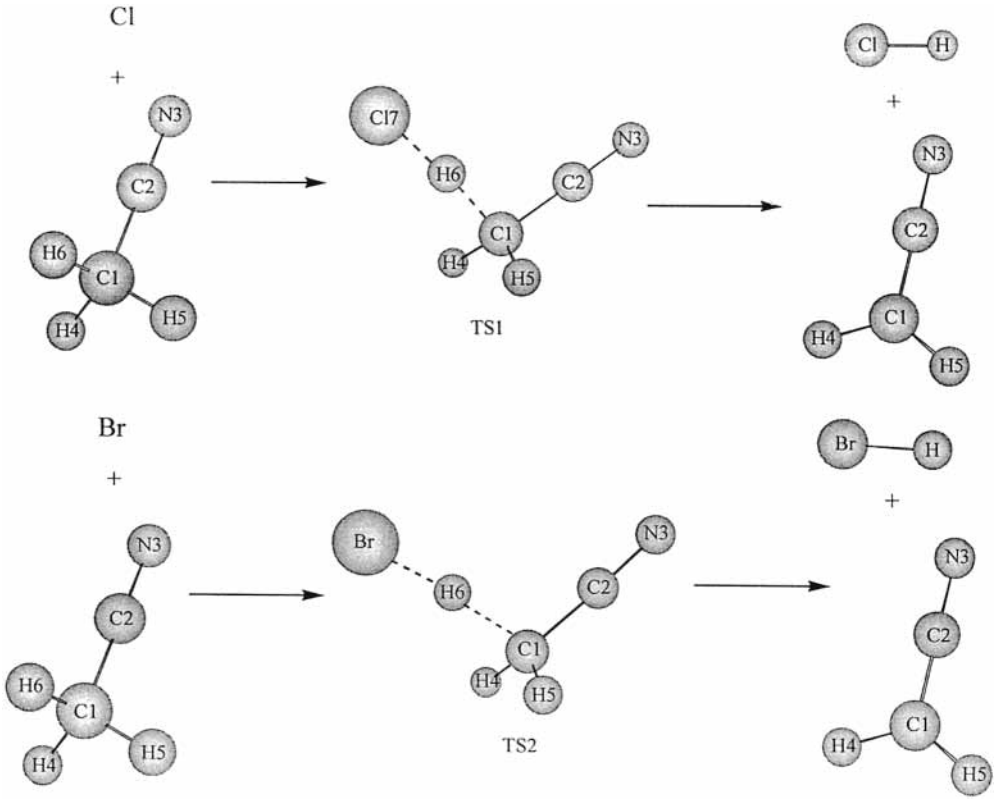

Figure 1. Optimized geometric structures of the reactants, products, and transition states.

TABLE 2: Reaction Energies and Barrier Heights (in kcal mol^{-1}) of the CH_3CN + Cl and CH_3CN + Br Reactions[a]

methods	ΔE	$\Delta H_{0K}{}^0$	$\Delta H_{298K}{}^0$	$V^{\ddagger}$	$V_a{}^{G\ddagger}$
		$CH_3CN+Cl=CH_2CN+HCl$[a]			
BH&HLYP/6-311G(d, p)	−1.18	−6.18	−5.57	10.80	6.29
BH&HLYP/6-31+G(d, p)	0.15	−4.82	−4.21	11.82	7.34
MP2/6-311G(d, p)	9.41	5.89	6.47	18.82	15.85
MP2/6-31+G(d, p)	12.21	8.68	9.23	21.71	18.82
QCISD/6-311G(d, p)	0.27	−4.57	−3.95	13.76	9.32
Single-point energy calculations					
BH&HLYP/6-311++G(3df, 2p)// BH&HLYP/6-311G(d, p)	−2.87	−7.88	−7.26	9.87	5.36
QCISD/6-311++G(d, p)// MP2/6-311G(d, p)	0.71	−2.81	−2.23	12.81	9.93
QCISD(T)/6-311G(d, p)// MP2/6-311G(d, p)	1.83	−1.70	−1.12	13.11	10.14
CCSD(T)/cc-pVTZ// QCISD/6-311G(d, p)	−0.83	−5.68	−5.05	10.32	5.88
G2//MP2/6-311G(d, p)	−7.41		−6.83	6.65	
		$CH_3CN+Br=CH_2CN+HBr$[b]			
BH&HLYP/6-311G(d, p)	11.27	6.05	6.41	18.62	13.63
Single-point energy calculations					
BH&HLYP/6-311++G(3df , 2p) //BH&HLYP/6-311G(d, p)	10.30	4.87	5.23	16.32	11.33
G2	6.84		6.83	13.05	

[a] Standard reaction enthalpies[39]: -8.31 ± 8.97 kcal mol^{-1}; 7.31 ± 8.97 kcal mol^{-1}. Experimental activation energies: $\approx$6.0 kcal mol^{-1} in 370.5−413 K[11]; 5.52 kcal mol^{-1} in 478−713 K[12]; >3.97 kcal mol^{-1} at 298 K[13]; 4.24 kcal mol^{-1} in 274.5−345.5 K.[10] ΔE: Reaction energy; $\Delta_r H_{0\ K^\circ}$: Calculated standard reaction enthalpy at 0 K; $\Delta_r H_{298\ K^\circ}$: Calculated standard reaction enthalpy at 298 K; $V^{\ddagger}$: Classical barrier height; $V_a{}^{G\ddagger}$: $V^{\ddagger}$ corrected with the zero-point energy.

method (5.88 kcal mol^{-1}). In the next section, we will show that the fitted activation energies from ICVT/SCT rate constants using these values are close to the experimental data. However, the barrier heights calculated using MP2 method and those calculated based on MP2 geometries are generally overestimates. So the reaction energies and barrier heights predicated at the BH&HLYP/6-311++G(3df, 2p)//BH&HLYP/6-311G(d, p) level of theory are deemed to be reasonable for the reactions discussed here.

The harmonic vibrational frequencies and the zero-point energies (ZPE) for the reactant (CH_3CN), products (CH_2CN, HCl), and the transition state ($NCH_2C^1\cdots H^6\cdots Cl^7$) calculated by different theoretical methods along with some available experimental data[40,41] are listed in Table 3. For CH_3CN, CH_2CN, and HCl species, the calculated frequencies agree well with the experimental data except for the stretching mode C^2-N^3 (2266 cm^{-1}) and bending mode C^1-C^2-N^3 (362 cm^{-1}). In the transition state $NCH_2C^1\cdots H^6\cdots Cl$,[7] the calculated real frequencies at the

TABLE 3: Calculated and Experimental Frequencies (in cm^{-1}) and ZPE (in kcal mol^{-1}) at the Stationary Points

	BH&HLYP		MP2		QCISD	
	6-311G(d, p)	6-31+G(d, p)	6-311G(d,p)	6-31+G(d, p)	6-311G(d, p)	exptl
CH_3CN	3217	3217	3195	3245	3166	3009[b]
	3140	3140	3101	3143	3082	2954[a]
	2489	2489	2218	2218	2343	2266[a]
	1527	1527	1501	1522	1503	1448[a]
	1466	1466	1428	1455	1436	1381[a]
	1104	1104	1073	1082	1078	1041[a]
	959	959	936	938	930	920[a]
	407	399	367	334	374	362[a]
ZPE	29.40	29.47	28.53	28.76	28.63	
CH_2CN	3354	3388	3374	3429	3310	3301[b]
	3252	3276	3246	3297	3196	
	2209	2209	2754	2757	2133	2156[b]
	1494	1503	1471	1499	1470	
	1079	1084	1076	1095	1046	1124[b]
	1073	1075	1020	1030	1034	1041[b]
	683	687	576	564	607	680[b]
	459	445	452	444	424	437[b]
	408	400	429	421	377	367[b]
ZPE	20.05	20.11	20.59	20.78	19.44	
HCl	3043	3068	3088	3112	3045	2991[a]
ZPE	4.35	4.39	4.41	4.45	4.35	
$NC_2H_2\cdots H\cdots Cl$	3294	3317	3288	3359	3239	
	3201	3220	3185	3241	3146	
	2379	2375	3105	3006	2264	
	1492	1497	1467	1489	1467	
	1230	1232	1195	1212	1209	
	1141	1142	1107	1105	1118	
	1021	1024	989	1001	1001	
	1011	1019	932	785	983	
	931	935	861	771	914	
	449	450	480	474	421	
	414	416	461	433	382	
	396	360	419	411	375	
	350	306	303	319	315	
	98	99	82	70	90	
	1524*i*	1562*i*	1570*i*	1003*i*	1669*i*	
ZPE	24.89	24.99	25.55	25.88	24.20	

[a] ref 40. [b] ref 41. Calculated frequencies at the BH&HLYP/6-311G(d, p) level of theory: HBr: 2721; $NC_2H_2\cdots H\cdots Br$: 3317 3216 2336 1492 1192 1106 1029 878 840 442 409 387 343 84 1182*i*. ZPE=24.42 kcal mol^{-1}; HBr: 2721. ZPE=3.89 kcal mol^{-1}.

BH&HLYP level differ from the QCISD/6-311G(d, p) results by at most 10% with the difference of 9 cm^{-1}. However, the MP2 results differ from QCISD/6-311G(d, p) results by 27% with the difference of 841 cm^{-1}. This is encouraging because the BH&HLYP method is computationally much less expensive than the MP2 and QCISD methods. The most noticeable discrepancy in the transition state frequencies calculated at different levels is the appearance of imaginary values. The imaginary values of vibrational frequencies depend strongly on the barrier height.[18] The BH&HLYP/6-311G(d, p) and BH&HLYP/6-31+G(d, p) imaginary frequencies are 145 and 107 cm^{-1} less than the QCISD/6-311G(d, p) value, respectively. This may be because BH&HLYP/6-311G(d, p) and BH&HLYP/6-31+G(d, p) classical barrier heights are 3.03 and 1.98 kcal mol^{-1} lower than the QCISD/6-311G(d, p) value. It can be seen that the imaginary values obtained using the MP2/6-311G(d, p) and MP2/6-31+G(d, p) methods are 99 and 666 cm^{-1} less than that of QCISD. However, the MP2/6-311G(d, p) and MP2/6-31+G(d, p) barrier heights are 5.06 and 7.95 kcal mol^{-1} higher than the QCISD/6-311G(d, p) results. So, for the frequencies calculated, the BH&HLYP method is seen to be more reasonable than the MP2 method.

From the discussion above, although some errors still remain in calculating the enthalpy of reaction and barrier height for the reaction $CH_3CN + Cl = CH_2CN + HCl$, the BH&HLYP/6-311G(d, p) method predicts more accurate geometries and frequencies for the stationary points. Furthermore, the barrier height and reaction enthalpy refined at the BH&HLYP/6-311++G(3df, 2p)//BH&HLYP/6-311G(d, p) level of theory are in satisfactory agreement with the higher level of theory results. Thus, in the present work, the BH&HLYP/6-311G(d, p) approach is used to calculate the geometries and frequencies along the MEPs and a series of single-point BH&HLYP/6-311++G(3df, 2p) calculations is performed to correct the energies. The reaction $CH_3CN + Br$ is similar to $CH_3CN + Cl$, and we might expect that the geometries, frequencies, and barrier heights could have the similar accuracy for the BH&HLYP method.

B. Reaction Path Properties. Changes of bond distances along the MEPs of the reactions $CH_3CN + Cl$ and $CH_3CN + Br$ are shown, respectively, in Figure 2a,b, which displays the $C^1\cdots H^6$ and $H^6\cdots Cl^7$/$H^6\cdots Br^7$ bond distances changing dramatically as functions of the intrinsic reaction coordinate *s*. In Figure 2a, as the reaction proceeds toward the products (i.e., *s* changes from $-\infty$ to $+\infty$), the $C^1\cdots H^6$ bond distance remains practically invariant until the reaction coordinate *s* reaches about -0.4 $(amu)^{1/2}$ bohr, where it starts to elongate almost linearly with *s* increasing, and the $H^6\cdots Cl^7$ bond distance also starts to shorten synchronously, and almost linearly, until *s* reaches about $+0.5$ $(amu)^{1/2}$ bohr. When $s > +0.5$, the $H^6\cdots Cl^7$ bond distance only experiences a small change. The points where these marked changes take place show that the beginning of the dissociation of the $C^1\cdots H^6$ bond and the end of the formation of $H^6\cdots Cl^7$ bond, respectively. It can be seen that the geometric changes

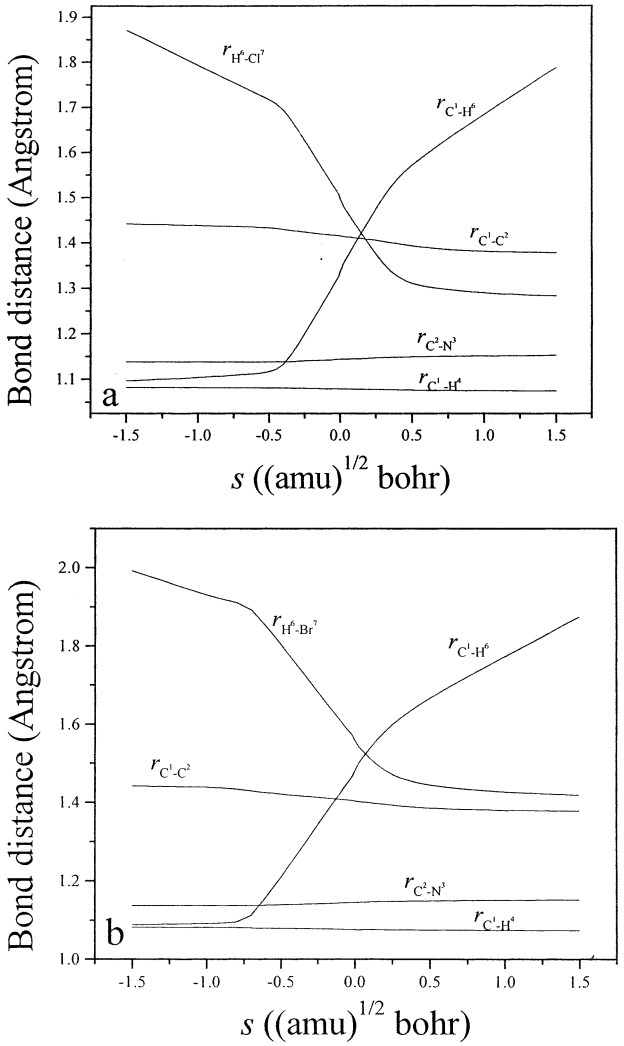

Figure 2. Changes of the bond distances (in Å) as functions of s (amu)$^{1/2}$ bohr at the BH&HLYP/6-311G(d, p) level. (a) The CH_3CN + Cl reaction; (b) the CH_3CN + Br reaction.

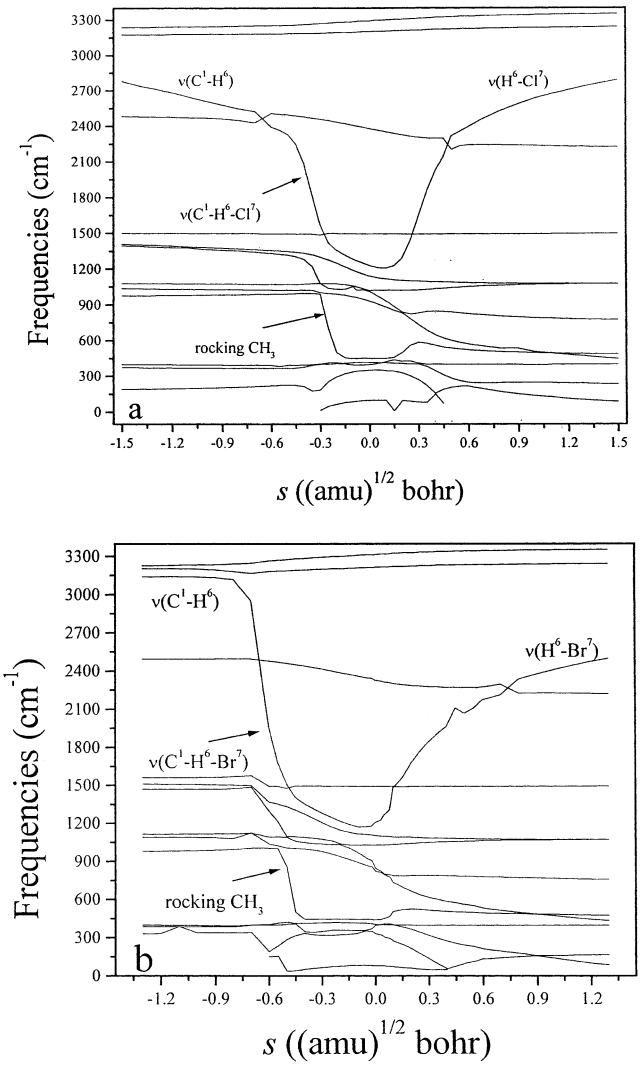

Figure 3. Changes of the generalized normal-mode vibration frequencies (in cm^{-1}) as functions of s (amu)$^{1/2}$ bohr at the BH&HLYP/6-311G(d, p) level. (a) The CH_3CN+ Cl reaction; (b) the CH_3CN + Br reaction.

take place mainly in the region from about $s = -0.40$ to $+0.50$ (amu)$^{1/2}$ bohr. The characters of the bond distance changed in Figure 2b are similar to those in Figure 2a. The main region of s that the bond ($C^1\cdots H^6$) and ($H^6\cdots Br^7$) distances change sharply lies at about -0.75 to $+0.25$ (amu)$^{1/2}$ bohr.

At the BH&HLYP/6-311G(d, p) level, the curves of the generalized frequencies along the MEPs for the two reactions are plotted in Figure 3a,b. When $s = -\infty$, the vibrational frequencies correspond to the reactant (CH_3CN), and when $s = +\infty$, the vibrational frequencies correspond to the products (CH_2CN and HCl in Figure 3a and CH_2CN and HBr in Figure 3b). Figure 3 shows obviously that the vibrational frequenices $\nu(C^1\cdots H^6\cdots Cl^7)$ and $\nu(C^1\cdots H^6\cdots Br^7)$ change dramatically in almost the same regions of s as Figure 2, namely, from -0.40 to $+0.50$ (amu)$^{1/2}$ bohr for reaction CH_3CN + Cl, and from -0.75 to $+0.60$ (amu)$^{1/2}$ bohr for reaction CH_3CN + Br. In Figure 3a, when $s < 0$ (amu)$^{1/2}$ bohr, the vibrational mode $\nu(C^1\cdots H^6\cdots Cl^7)$ is related to the stretching vibrational mode of the $C^1\cdots H^6$ bond that would be broken; however, when $s > 0$ (amu$^{1/2}$) bohr, the vibrational mode $\nu(C^1\cdots H^6\cdots Cl^7)$ is related to the stretching vibrational mode of the $H^6\cdots Cl^7$ bond that would be formed. This characterization indicates that the vibrational mode $\nu(C^1\cdots H^6\cdots Cl^7)$ is related closely to the hydrogen abstraction reaction, so that the vibrational mode $\nu(C^1\cdots H^6\cdots Cl^7)$ can be referred to as "reaction mode". The rapid decrease of the rocking CH_3 group also has impact on the calculations of the rate constant.[22] The vibrational mode $\nu(C^1\cdots H^6\cdots Cl^7)$ and the rocking CH_3 could lower the barrier and thus would significantly enhance the reaction rate constants. In Figure 3b, the $\nu(C^1\cdots H^6\cdots Br^7)$ "reaction mode" has a similar character to the vibrational mode $\nu(C^1\cdots H^6\cdots Cl^7)$.

The classical potential energy V_{MEP} (s) and the ground-state adiabatic potential energy V_a^G(s) as functions of the intrinsic reaction coordinate s are plotted in Figure 4. In Figure 4a, the curve V_a^G looks slightly different from the curve V_{MEP} in shape. There is a local maximum value near $s = -0.40$ (amu)$^{1/2}$ bohr in the curve V_a^G. A two-barrier shape of V_a^G, which was also found for $CH_3 + D_2$, CH_3 + HC, and CH_3F + Cl reactions,[42,43] implies that the variational effect may be significant on the calculations of the rate constants of the reaction CH_3CN + Cl. In Figure 4b, the shapes of the curves V_a^G and V_{MEP} are very similar to those for the reaction CH_3CN + Br, which implies that the variational effect on the calculations of the rate constants are not significant. To understand deeply the variational effect, the dynamic bottleneck properties of the two reactions based on the canonical variational transition state (CVT) approach are listed in Table 4, which shows the position s of the variational transition state at various temperatures is shifted from the saddle point $s = 0$. For the reaction CH_3CN + Cl, the maximum of

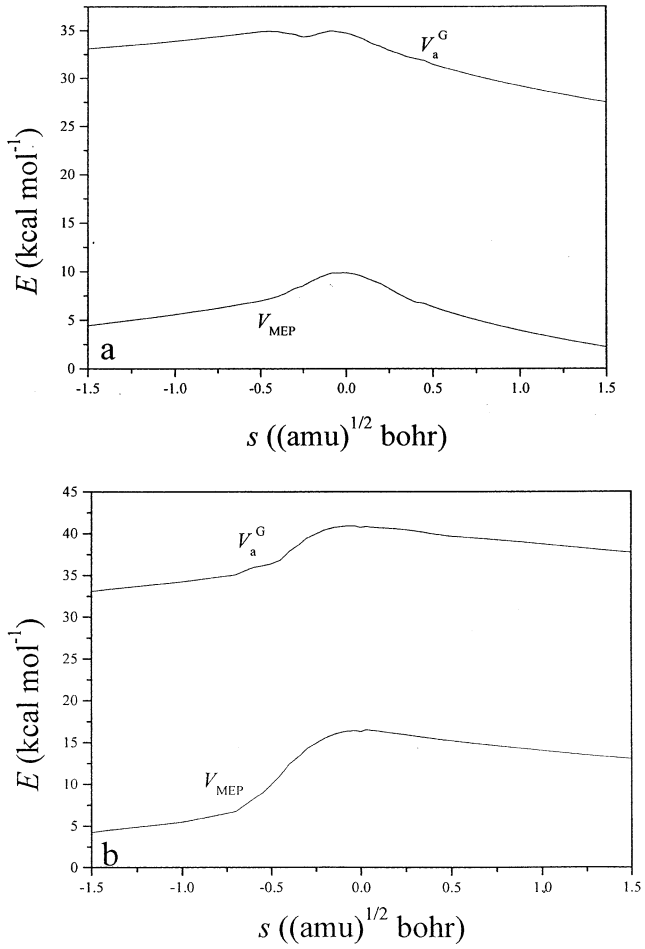

Figure 4. Classical potential energies (V_{MEP}) and ground-state adiabatic potential energies (V_a^G) (in kcal mol^{-1}) as functions of s (amu)$^{1/2}$ bohr at the BH&HLYP/6-311++G(3df, 2p)//BH&HLYP/6-311G(d, p) level. (a) The CH_3CN + Cl reaction; (b) the CH_3CN + Br reaction.

TABLE 4: Bottleneck Properties of the Reactions Based on the CVT Method

T (K)	s (bohr)	V_{MEP} (kcal)	V_a^G (kcal)
	$CH_3CN + Cl = CH_2CN + HCl$		
S.P.	0.000	9.87	34.76
250	−0.077	9.86	34.95
298	−0.076	9.87	34.95
500	−0.070	9.87	34.94
1000	−0.061	9.87	34.92
1500	−0.056	9.87	34.91
2000	−0.054	9.87	34.91
2500	−0.053	9.87	34.90
	$CH_3CN + Br = CH_2CN + HBr$		
S.P.	0.000	16.32	40.74
250	−0.049	16.42	40.92
298	−0.048	16.42	40.92
500	−0.047	16.42	40.92
1000	−0.047	16.42	40.92
1500	−0.048	16.42	40.92
2000	−0.049	16.42	40.92
2500	−0.050	16.42	40.92

shifted s is −0.077 (amu)$^{1/2}$ bohr at 250 K, where the values of the $V_{MEP}(-0.077)$ and $V_a^G(-0.077)$ are 9.86 and 34.95 kcal mol^{-1}, respectively. The differences, $V_{MEP}(s = -0.077) - V_{MEP}(s = 0) = -0.01$ kcal mol^{-1}, and $V_a^G(s = -0.077) - V_a^G(s = 0) = 0.19$ kcal mol^{-1}, are small. For the reaction CH_3CN + Br, the corresponding maximum value of shifted s is −0.050 (amu)$^{1/2}$ bohr, and the differences, $V_{MEP}(s = -0.050) - V_{MEP}(s = 0) = 0.01$ kcal mol^{-1}, and $V_a^G(s = -0.050) - V_a^G(s = 0) =$ 0.18 kcal mol^{-1}, are also small. This indicates that the variational effect on the rate constant calculations in the two reactions is not significant.

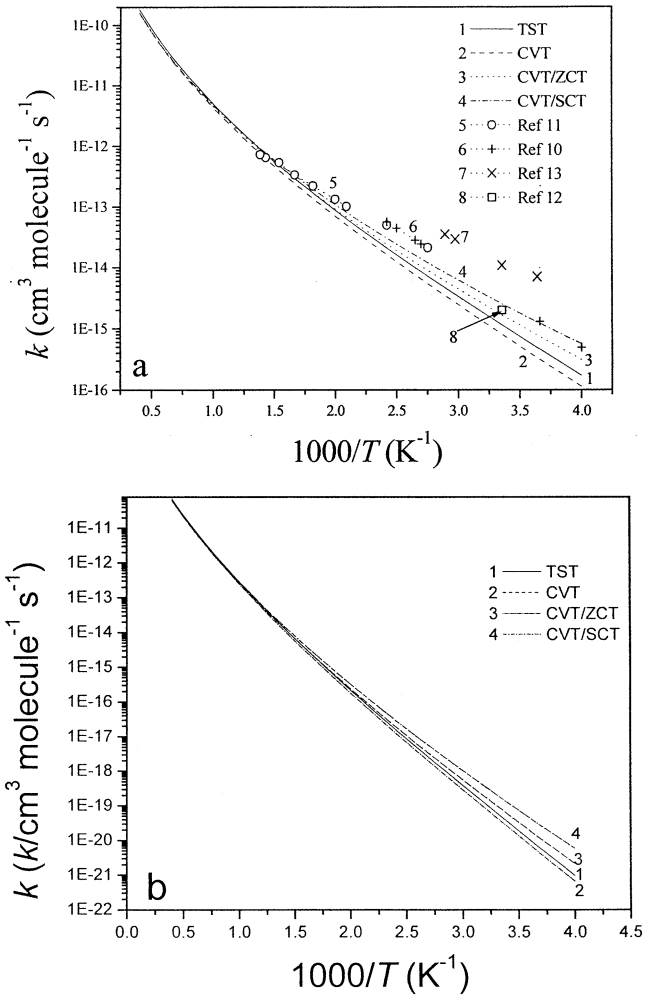

Figure 5. Forward reaction rate constants k (in cm^3 molecule^{-1} s^{-1}) as functions of the reciprocal of the temperature (K^{-1}) in the temperature range of 250−1500 K. (a) The reaction of CH_3CN with Cl; (b) the reaction of CH_3CN with Br.

C. Rate Constants. Calculated rate constants for the reactions CH_3CN + Cl and CH_3CN + Br are summarized in Table 5, along with some available experimental rate constants. The corresponding Arrhenius plots for the theoretical and experimental rate constants are shown in Figure 5. As shown in Figure 5a, TST and CVT rate constants are quite close to each other in the whole temperature range, again indicating that the variational effect is insignificant in the calculations of the rate constant. The TST, CVT, CVT/ZCT, and CVT/SCT rate constants are in good agreement with the experimental values at temperatures up to 500 K. And the CVT/SCT rate constants are in good agreement with the experimental values measured by Poulet et al.[11] and Olbregts et al.[10] in the temperature range of 360−723 K. The TST, CVT, and CVT/ZCT rate constants deviate substantially from the experimental values at temperatures lower than 500 K. In particular, the CVT/ZCT rate constants are obviously smaller than the CVT/SCT rate constants, indicating that the ZCT correction underestimates the tunneling contribution. From Table 5, it can be seen that Wigner tunneling corrections are comparable with the small-curvature tunneling correction results. To obtain better accuracy, it is necessary to perform large-curvature tunneling (LCT) calculations, which need to compute information of the global potential

TABLE 5: Calculated and Experimental Forward Rate Constants (in cm^3 Molecule^{-1} s^{-1}) for the Two Reactions

T (K)	TST	TST/W	CVT	CVT/ZCT	CVT/SCT	exptl[a]
			$CH_3CN + Cl = CH_2CN + HCl$			
250.0	1.72E−16	7.23E−16	1.13E−16	3.39E−16	2.10E−15	4.90E−16[a]
273.0	4.59E−16	1.69E−15	3.12E−16	7.83E−16	3.14E−15	1.30E−15[a]
274.5	4.87E−16	1.78E−15	3.32E−16	8.24E−16	3.22E−15	7.00E−15[b]
298.0	1.03E−15	3.72E−15	7.22E−16	1.59E−15	4.70E−15	
336.0	1.14E−15	1.00E−14	8.02E−16	1.74E−15	4.98E−15	3.49E−14[b]
345.5	3.61E−15	1.25E−14	2.65E−15	4.88E−15	1.01E−14	3.49E−14[b]
363.0	4.65E−15	1.82E−14	3.44E−15	6.14E−15	1.20E−14	2.11E−14[c]
370.5	8.59E−15	2.11E−14	6.47E−15	1.07E−14	1.86E−14	1.30E−14[a]
400.0	1.62E−14	3.66E−14	1.25E−14	1.92E−14	3.01E−14	5.10E−14[a]
478.0	6.34E−14	1.19E−13	5.04E−14	6.82E−14	9.10E−14	1.01E−13[c]
723.0	8.98E−13	1.24E−12	7.52E−13	8.53E−13	9.57E−13	7.25E−13[c]
800.0	1.58E−12	2.07E−12	1.33E−12	1.47E−12	1.61E−12	
1000.0	4.94E−12	5.93E−12	4.23E−12	4.48E−12	4.75E−12	
			$CH_3CN + Br = CH_2CN + HBr$			
250.0	9.75E−22	2.85E−21	6.61E−22	2.15E−21	5.94E−21	
298.0	4.58E−20	1.08E−19	3.30E−20	7.55E−20	1.60E−19	
400.0	8.85E−18	1.55E−17	6.88E−18	1.09E−17	1.71E−17	
500.0	2.21E−16	3.27E−16	1.79E−16	2.41E−16	3.26E−16	
600.0	2.08E−15	2.78E−15	1.73E−15	2.13E−15	2.64E−15	
700.0	1.11E−14	1.38E−14	9.41E−15	1.09E−14	1.29E−14	
800.0	4.09E−14	4.86E−14	3.52E−14	3.95E−14	4.48E−14	
1000.0	2.81E−13	3.15E−13	2.47E−13	2.65E−13	2.88E−13	

[a] ref 11. [b] ref 10. [c] ref 12.

TABLE 6: Fitted Forward Activation Energies (in kcal mol^{-1}) for the Two Reactions

low T	high T	TST	CVT	CVT/ZCT	CVT/SCT
		$CH_3CN + Cl = CH_2CN + HCl$			
250.0	363.0	5.97	6.17	5.26	4.89
274.5	345.5	5.99	6.21	5.33	4.97
295.0	478.0	6.31	6.50	5.76	5.43
295.0	723.0	6.70	6.88	6.23	5.93
370.5	413.0	6.40	6.58	5.88	5.56
478.0	723.0	7.43	7.58	7.08	6.83
800.0	1500.0	9.99	10.07	9.80	9.64
1500.0	2500.0	13.58	13.63	13.50	13.41
		$CH_3CN + Br = CH_2CN + HBr$			
250.0	363.0	12.00	12.19	11.19	10.42
274.5	345.5	12.04	12.22	11.26	10.52
295.0	478.0	12.38	12.55	11.75	11.09
295.0	723.0	12.80	12.97	12.28	11.67
370.5	413.0	12.47	12.65	11.90	11.26
478.0	723.0	13.59	13.75	13.24	12.74
800.0	1500.0	16.26	16.40	16.11	15.81
1500.0	2500.0	19.93	20.05	19.90	19.72

surface. Obviously, this deserves to be studied further. For the reaction $CH_3CN + Br$, although no experimental data are available for comparison, the rate constants might be predicted to have accuracy similar to the reaction $CH_3CN + Cl$.

The calculated Arrhenius average activation energies of the two reactions for several temperature ranges are listed in Table 6. The experimental activation energies of the reaction $CH_3CN + Cl$ at various temperatures have been reported by several authors. They are >3.97 kcal mol^{-1} at 298 K,[12] 6.0 kcal mol^{-1} at 413 K,[10] 4.24 kcal mol^{-1} in the range 274.5−345 K,[13] 3.0 kcal mol^{-1} at 300 K and 6.0 kcal mol^{-1} at 723 K.[11] Obviously, the fitted activation energies for the reaction $CH_3CN + Cl$ are in reasonable agreement with the experimental values in the measured temperature range of 250−723 K. In any of the temperature ranges, the fitted activation energies for the reaction $CH_3CN + Br$ are all notably higher than that for the reaction $CH_3CN + Cl$.

4. Summary

We have performed a direct dynamics study on the reactions $CH_3CN + Cl = CH_2CN + HCl$ and $CH_3CN + Br = CH_2CN + HBr$. It was found that the BH&HLYP method with the 6-311G(d, p) basis set yields geometries and frequencies at the stationary points of comparable accuracy to those of the more computationally expensive QCISD/6-311G(d, p) level. Therefore, in the present paper, the BH&HLYP/6-311G(d, p) method is settled on the calculation of the geometries and frequencies along withthe MEPs for the two titled reactions. More accurate barrier heights predicted at the BH&HLYP/6-311++G(3df, 2p)//BH&HLYP/6-311G(d, p) level are 5.36 kcal mol^{-1} for the reaction $CH_3CN + Cl$ and 13.03 kcal mol^{-1} for the reaction $CH_3CN + Br$, respectively.

By analyzing changes in the geometies and frequencies along the MEPs, it was found that the reaction regions are from about -0.40 to $+0.50$ (amu)$^{1/2}$ bohr for the reaction $CH_3CN + Cl$ and about -0.75 to $+0.25$ (amu)$^{1/2}$ bohr for the reaction $CH_3CN + Br$, including the breaking of $C^1\cdots H^6$ and the forming of $Cl^7\cdots H^6/Br^7\cdots H$.[6]

The rate constants and the activation energies were calculated in the temperature range of 200−2500 K by using the canonical variational transition-state theory incorporating zero-curvature tunneling and small-curvature tunneling corrections. For the reaction $CH_3CN + Cl$, the calculated forward reaction rate constants are in satisfactory agreement with the experimental values in the measured temperature range, and the fitted activation energies are in reasonable agreement with the corresponding experimental data. Calculations of the rate constants indicate that the variational effect on the rate constants is very small, and that the tunneling corrections are very important for the rate constant calculations in the low-temperature range. The rate constants are also predicted for the reaction $CH_3CN + Br$ at the same level. From these calculated rate constants, it can be ascertained that the reaction $CH_3CN + Cl$ plays a more important role than the reaction $CH_3CN + Br$ for the diminishment of CH_3CN in the stratosphere.

Acknowledgment. This work is supported by the National Science Foundation of China. We thank Professor D. G. Truhlar for providing the POLYRATE 8.2 program. We thank Dr. Y. M. Xie for his kind help. We are also grateful to our reviewers for their valuable comments on the manuscript.

References and Notes

(1) Arnold, F.; Krankosky, D.; Marien, K. H. *Nature (London)* **1977**, *167*, 30.
(2) Arijs, E.; Ingels, J.; Nevejans, D. *Nature (London)* **1978**, *271*, 642.
(3) Arijs, E.; Nevejans, D.; Ingels, J. *Nature (London)* **1980**, *288*, 684.
(4) Arnold, F.; Bohringer, F.; Henschen, G. *Geophys. Res. Lett*. **1978**, *5*, 653.
(5) Becker, K. H.; Ionescu, A. *Geophys. Res. Lett*. **1982**, *9*, 1349.
(6) Arijs, E.; Nevejans, D.; Ingels, J. *Nature (London)* **1983**, *303*, 314.
(7) Hamm, s.; Warneck, P. J. *Geophys. Res*. **1990**, *95*, 20593.
(8) Holzinger, R.; Warneke, C.; Hansel, A. *Geophys. Res. Lett*. **1999**, *26*, 1161.
(9) Brasseur, G.; Arijs, E.; De Rudder, A.; Nevejans, D.; Angels, J. *Geophys. Res. Lett*. **1983**, *10*, 725.
(10) Olbregts, J. Brasseur, G.; Arijs, E. *J. Photochem*. **1984**, *24*, 315.
(11) Poulet, G.; Laverdet, G.; Jourdain, J. L.; Le Bras, G. *J. Phys. Chem*. **1984**, *88*, 6259.
(12) Kurylo, M. J.; Knable, G. L. *J. Phys. Chem*. **1984**, *88*, 3305.
(13) Tyndall, G. S.; Orlando, J. J. *J. Phys. Chem*. **1996**, *100*, 660.
(14) Dobb, K. D.; Dixon, D. A. *J. Phys. Chem*. **1994**, *98*, 12584.
(15) Troung, T. N.; Duncan, W. *J. Chem. Phys*. **1994**, *101*, 7408.
(16) Bell, R. L.; Troung, T. N. *J. Chem. Phys*. **1994**, *101*, 10442.
(17) Troung, T. N. J. *Chem. Phys*. **1995**, *102*, 5335.
(18) Duncan, W. T.; Troung, T. N. *J. Chem. Phys*. **1995**, *103*, 9642.
(19) Becke, A. D. *J. Chem. Phys*. **1993**, *98*, 1372.
(20) Lee, C.; Yang, W.; Parr, R. G. *Phys. Rev. B* **1988**, *37*, 785.
(21) Møller, C.; Plesset, M. S. *Phys. Rev*. **1934**, *46*, 618.
(22) Head-Gordon, M.; Pople, J. A.; Frisch, M. J. *Chem. Phys. Lett*. **1988**, *153*, 503.
(23) Pople, J. A.; Head-Gordon, M.; Raghavachari, K. *J. Chem. Phys*. **1987**, *87*, 5968.
(24) Frisch, M. J.; Trucks, G. W.; Schlegel, H. B.; Scuseria, G. E.; Robb, M. A.; Cheeseman, J. R.; Zakrzewski, V. G.; Montgomery, J. A.; Stratmann, R. E.; Burant, J. C.; Dapprich, S.; Daniels, A. D.; Kudin, K. N.; Strain, M. C.; Farkas, O.; Tomasi, J.; Barone, V.; Cossi, M.; Cammi, R.; Mennucci, B.; Pomelli, C.; Adamo, C.; Clifford, S.; Ochterski, J.; Peterson, G. A.; Ayala, P. Y.; Cui, Q.; Morokuma, K.; Malik, D. K.; Rabuk, A.d.; Raghavachari, K.; Foresman, J. B.; Cioslowski, J.; Ortiz, J. V.; Stefanov, B. B.; Liu, G.; Liashenko, A.; Piskorz, P.; Komaromi, I.; Gomperts, R.; Martin, R. L.; Fox, D. J.; Keith, T.; Al-Laham, M. A.; Peng, C. Y.; Nanayakkara, A.; Gonzalez, C.; Chalacombe, M.; Gill, P. M. W.; Johnson, B. G.; Chen, W.; Wong, M. W.; Andres, J. L.; Head-Gordon, M.; Replogle, E. S.; Pople, J. A.; *Gaussian 98*; Gaussian Inc.: Pittsburgh, PA, 1998.
(25) Chuang, Y Y.; Corchado, J. C.; Fast, P. L.; Villà, J.; Hu, W.-P. Liu, Y. -P.; lynch, G. C.; Jackels, C. F.; Nguyen, K. A.; Gu, M. Z.; Rossi, I.; Isaacson, E. L.; Truhlar, D. G. *Polyrate*, version 8.2; University of Monnesota: Minneapolis, 1999.
(26) Truhlar, D. G.; Isaacson, A. D.; Garrett, B. C. In *The Theory of Chemical Reaction Dynamics*; Baer, M., Ed. CRC Press: Boca Raton, FL, 1985; Vol. 4, p 65.
(27) Truhlar, D. G.; Kuppermann, A. *J. Chem. Phys*. **1970**. *52*, 3842;
(28) Garrett, B. C.; Truhlar, D. G.; Grev, R. S.; Magnuson, A. W. *J. Phys. Chem*. **1980**, *84*, 1730.
(29) Steckler, R.; Hu, W.-P.; Liu, Y.-P.; Lynch, G. C.; Garrett, B. C.; Isaacson, A. D.; Melssas, V. S.; Lu, D.-H.; Troung, T. N.; Rai, S. N.; Hancock, G. C.; Lauderdale, J. C.; Joseph, T.; Truhlar, D. G. *Comput. Phys. Commun*. **1995**, *88*, 491.
(30) Duncan, W. T.; Bell, R. L.; Troung, Y. N. *J. Comput. Phys*. **1998**, *19*, 1039.
(31) Truhlar, D. G.; Garrett, B. C.; Klippenstein, S. J. *J. Phys. Chem*. **1996**, *100*, 12771.
(32) Trong, T. N.; Truhlar, D. G. *J. Chem. Phys*. **1990**, *93*, 1761.
(33) Liu, Y.-P.; Lynch, G. C.; Truong, T. N.; Lu, D.-H.; Truhlar, D. G. *J. Am. Chem. Soc*. **1993**, *115*, 2408.
(34) Demaison, J.; Durbrulle, A.; Boucher, D.; Burie, J.; Typke, V. *J. Mol. Spectosc*. **1979**, *76*, 1.
(35) Lide, D. R. *CRC HandBook of Chemistry and Physics*, 73rd ed.; CRC: Boca Raton, FL, 1992−1993; Section 9.
(36) Saito, S.; Yamamoto, S. *J. Chem. Phys*. **1997**, *107*, 1732.
(37) Wang, B.; Hou, H.; Gu, Y. *J. Phys. Chem. A* **2001**, *105*, 156.
(38) Gutsev, G. L.; Sobolewski, A. L.; Adamowicz, L. *Chem. Phys*. **1995**, *196*, 1.
(39) Atkinson, R.; Baaulch, D. L.; Cox, R. A.; Hampson, R. F. Kerr, J. A.; Rossi, M. J.; Troe, J. *J. Phys. Chem. Ref. Data*; Supplement VII, Appendix 1, 1999.
(40) Koga, Y.; Hondo, S.; Saeki, S.; Person, W. B. *J. Phys. Chem*. **1984**, *88*, 3152.
(41) Sumiyoshi, Y.; Tanaka, K.; Tanaka, T. *J. Chem. Phys.* **1996**, *104*, 1839.
(42) Rosenman, E.; McKee, M. L. *J. Am. Chem. Soc*. **1997**, *119*, 9033.
(43) Corchado, J. C.; Espinosa-Garcia, J. *J. Chem. Phys*. **1997**, *106*, 4013.